Available online at www.sciencedirect.com
ScienceDirect
Journal of Colloid and Interface Science 303 (2006) 557–563
JOURNAL OF Colloid and Interface Science
www.elsevier.com/locate/jcis

Formation and stability of paraffin oil-in-water nano-emulsions prepared by the emulsion inversion point method

Weirong Liu, Dejun Sun *, Caifu Li, Qian Liu, Jian Xu

Key Laboratory for Colloid and Interface Chemistry of Education Ministry, Shandong University, Jinan, Shandong 250100, People's Republic of China

Received 10 June 2006; accepted 23 July 2006

Available online 26 July 2006

Abstract

Paraffin oil-in-water nano-emulsions stabilized by Tween 80/Span 80 were prepared using the emulsion inversion point method at different emulsification temperatures. Nano-emulsions with droplet size below 200 nm were formed above a critical surfactant-to-oil ratio of 0.20 at 50 °C. The main destabilization mechanism of the systems was found to be Ostwald ripening. An interesting phenomenon was that the Ostwald ripening rate declined as the surfactant concentration rose. Furthermore, flocculation was also found to contribute to the instability of the nano-emulsions, especially for those with low surfactant concentrations. Study on the electrophoretic properties of emulsion droplets revealed a negative value of the zeta potential, which was strongly dependent on the pH of the systems.

Keywords: Nano-emulsions; Emulsion inversion point; HLB; Long-term stability; Ostwald ripening; Zeta potential

1. Introduction

Since the 1980's, attention has been focused on emulsions with droplet size in the nanometer range, which are referred to as nano-emulsions [1,2], miniemulsions [3,4], fine-disperse emulsions [5], homogeneous emulsions [6], submicron emulsions [7], or unstable microemulsions [8]. Due to their small size, nano-emulsions often possess long-term physical stability, showing properties superior to the conventional emulsions. On the other hand, compared with microemulsions, nano-emulsions can be prepared using moderate surfactant concentrations, which has great attraction for practical applications in many fields, such as cosmetics [9], pharmaceuticals [10], miniemulsion polymerization [3,4], and so forth.

According to the literatures, nano-emulsions can be prepared by high-energy [11,12] or low-energy emulsification methods [13–16]. High-energy emulsification methods require large mechanical energy generated by high-pressure homogenizers or ultrasound generators to produce fine droplets. In contrast, low-energy emulsification methods can take advantage of the chemical energy stored in the ingredients and produce the nano-emulsions almost spontaneously, thus have great attraction both in theoretical study and practical application. The change in the spontaneous curvature of surfactants during the emulsifying process has been recognized to be a key factor for the formation of nano-emulsions, which can be achieved either by changing the temperature (phase inversion temperature, PIT method) [13,14] or by changing the volume fraction of water or oil (emulsion inversion point, EIP method) [15,16].

Paraffin oil has been applied in many fields as a component of O/W emulsions, mostly as macroemulsions. The formation of paraffin oil emulsions with submicron droplets using the EIP method has occasionally been reported. Sagitani et al. [6] suggested that a proper HLB value of the surfactants was a key factor for the formation of emulsion with minimal droplets. Dai et al. [17] observed that the molecular structure of emulsifiers had a great effect on the droplet size of the final emulsions. Fernandez et al. [16] attained paraffin oil nano-emulsions with droplet sizes of 300–500 nm with surfactant-to-oil weight ratios of 0.364 and 0.5 at 80 °C.

In the present work, we obtained paraffin oil-in-water nano-emulsions at different emulsification temperatures using the EIP method. Nano-emulsions with droplet size below 200 nm

* Corresponding author. Fax: +86 531 88564750.
E-mail address: djsun@sdu.edu.cn (D. Sun).

0021-9797/$ – see front matter
doi:10.1016/j.jcis.2006.07.055

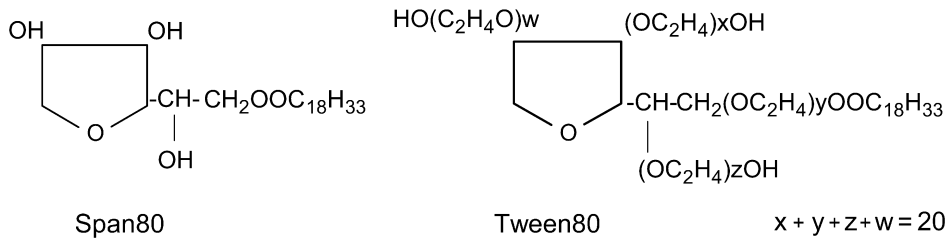

Fig. 1. The structures of Span 80 and Tween 80.

Table 1
Summary of some physical properties of Tween 80 and Span 80

	HLB	M_W (g mol^{-1})	A (nm^2)
Span 80	4.3	429	0.46
Tween 80	15.0	1310	2.48

Note. The values for Span 80 are from Ref. [24], and the values for Tween 80 are from Ref. [25]. HLB (hydrophilic–lipophilic balance), M_W (molecular weight), A (molecular area).

above a critical surfactant-to-oil ratio of 0.20 were obtained at 50 °C. We found that the main destabilization process for the systems was Ostwald ripening. However, the Ostwald ripening rate decreased with increasing surfactant concentration, in contrast to the results of many other researchers [13,18–20].

2. Materials and methods

2.1. Materials

Paraffin oil ($\rho = 0.845$ g cm^{-3}, c.p.) was a product of Lianhua Chemical Reagent Co., China. Sorbitan monooleate (Span 80, c.p.), polyoxyethylene (20) sorbitan monooleate (Tween 80, c.p.), hydrochloric acid (HCl, a.p.) and sodium hydroxide (NaOH, a.p.) were obtained from Tianjin Kermel Chemical Reagent Development Centre, China. The structures of Tween 80 and Span 80 were presented in Fig. 1. Some physical properties of Tween 80 and Span 80 were listed in Table 1. All reagents were used as received without further purification. Water used in this work was deionized water.

2.2. Methods

2.2.1. Preparation of emulsions

Emulsions were prepared from a mixture of paraffin oil and surfactants by slowly adding water with gentle agitation using a magnetic stirrer. The addition rate of water was kept constant at approximately 1.0 ml min^{-1}. The emulsification temperatures were kept at 30, 40 and 50 °C, respectively. The concentration of paraffin oil in all emulsions was kept constant at 20.0 wt%, while the surfactant concentration was varied from 3.0 to 8.0 wt%.

2.2.2. Droplet size determination

Emulsion droplet size and size distribution were determined by dynamic laser light scattering (DLS), using a Brookhaven Instrument (BI-200SM). An argon laser ($\lambda = 488$ nm) with variable intensity was used to cover the size range involved. Measurements were carried out at 25 °C with a scattering angle of 90°. Just before the measurement, the sample was prepared by diluting the emulsion about 1000 times with deionized water. Intensity averaged radii were computed from the intensity autocorrelation data with the cumulants method. And the intensity-intensity time correlation functions were analyzed by the CONTIN method [21].

2.2.3. Long-term stability

The long-term stability of nano-emulsions was assessed by measuring the droplet size as a function of time. The samples were kept sealed at room temperature.

2.2.4. Electrophoretic properties

The electrophoretic properties of emulsion droplets were determined using a DXD-II microelectrophoresis instrument (Jiangsu optical instrument Co., China). The values of the zeta potential were calculated by Smoluchowski's formula:

$$\zeta = \frac{4\pi\eta}{\varepsilon}\frac{\upsilon}{U/L}, \tag{1}$$

where η and ε are the viscosity and dielectric constant of water, respectively, υ is the mobile velocity of the oil droplets in the electric field, U is the voltage and L is the distance between the two electrodes.

The pH of the samples was determined with a pHS-25 pH meter (Leici Co., China). And the pH was adjusted with small volumes of 0.01 M NaOH or 0.01 M HCl. The experiments were carried out at 25 °C.

3. Results and discussion

3.1. Optimum HLB values

The emulsions were prepared using a mixture of the nonionic surfactants Tween 80 and Span 80. The mixing ratios were adjusted to satisfy the proper HLB values for optimum emulsification conditions. The mixed HLB values were calculated by the following equation:

$$\mathrm{HLB_{mix}} = \mathrm{HLB}_T\,\mathrm{T\%} + \mathrm{HLB}_S\,S\%, \tag{2}$$

where HLB_T, HLB_S and $\mathrm{HLB_{mix}}$ are the HLB values of Tween 80 (15.0), Span 80 (4.3) and the mixed surfactants, and T% and S% are the mass percentages of Tween 80 and Span 80 in the mixed surfactants, respectively. All the HLB values used were obtained at 25 °C.

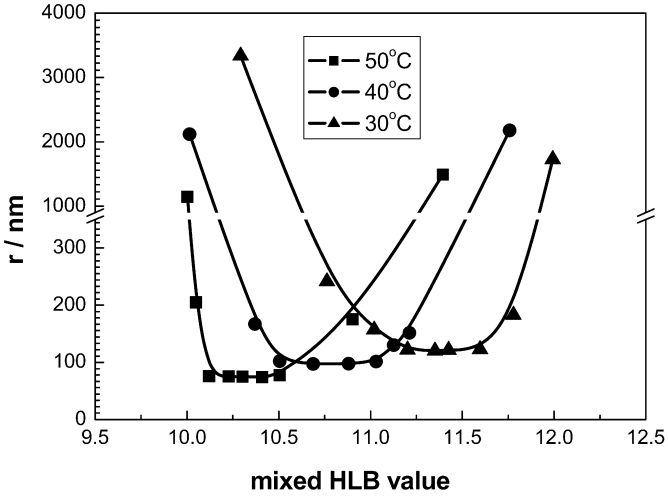

Fig. 2. Radius of droplet as a function of the mixed HLB values for samples with 20.0 wt% paraffin oil and 5.0 wt% surfactants at different temperatures.

Emulsions with 20.0 wt% paraffin oil and 5.0 wt% surfactants at different surfactant mixing ratios were prepared at different temperatures (30, 40 and 50 °C). The relationship between the droplet size of the obtained emulsions and the HLB values is shown in Fig. 2. First, we can see that emulsions with droplet diameters below 300 nm were obtained at these three temperatures by adjusting the HLB values of the surfactants. The formation of paraffin oil-in-water nano-emulsions at low emulsification temperatures may make them more attractive in the practical applications. Second, there is a narrow HLB region corresponding to the minimum droplet size at each temperature, beyond which the droplet size increases sharply. Within the optimum HLB regions, a transparent liquid crystalline phase (as determined by observation through a polarizer) and later a viscous white gel phase appear in the emulsifying process, in agreement with the results in the literatures [6,17]. The liquid crystalline phase corresponds to the lowest interfacial tension and the maximal solubilization of oil [6,24]. This is similar to the existence of bicontinuous microemulsion at the phase inversion temperature. Shinoda et al. [14]reported that the droplet size of O/W emulsion and the interfacial tension had a minimum at the PIT range. Morales et al. [25] showed that the main requirement for the formation of bluish transparent nano-emulsions was the complete solubilization of the oil component in the bicontinuous microemulsion. The following viscous gel phase was suggested to be an oil-in-surfactant emulsion [6]. The high viscosity of the gel phase could prevent coalescence between oil droplets and help the droplets disperse uniformly.

Also we can see from Fig. 2 that the optimum HLB values decrease with increasing temperature. It is well known that the HLB values of nonionic surfactants decrease with increasing temperature. Hence the actual HLB values at higher temperature should be smaller than that calculated from Eq. (2). That is to say, in order to maintain the actual HLB values, the calculated HLB values should increase as the temperature increases. So we conclude that the HLB value is not the only determining factor for the formation of nano-emulsions. We think the reduction of the optimum HLB values may be attributed to the polydispersity of the hydrophilic surfactant Tween 80 used in the experiments. This may be similar to the decrease of PIT with increasing surfactant concentration [25]. There is a wide distribution of EO units in the molecules of Tween 80, the molecules of Tween 80 with higher EO content preferentially partition into water. As the temperature increases, the hydrophilicity of molecules with higher EO content decreases, which tend to adsorbing to the interface between the paraffin oil and water. As a result, the ratio of Tween 80 in the interface increases with increasing temperature, which makes the interface film more hydrophilic and hence promotes the formation of O/W emulsions.

Table 2
Minimum radius, r_{min}, for samples with 20.0 wt% paraffin oil and 5.0 wt% surfactants prepared at different temperatures

T (°C)	30	40	50
r_{min} (nm)	120	98	74

In addition, the minimum radius decreased from 120 to 74 nm as the emulsification temperature increased from 30 to 50 °C, as shown in Table 2. This may be interpreted by the decrease of the oil viscosity and hence decreased cohesion forces between oil molecules with increasing temperature, which leads to smaller droplets [26].

3.2. The effect of surfactant concentrations

As stated above, nano-emulsions with droplet size below 200 nm can be obtained at 50 °C in a HLB region of 10.1–10.5. Here we select nano-emulsions prepared at 50 °C with a constant HLB number (10.3, with the weight ratio of Span 80/Tween 80 approximately 0.44/0.56) to investigate the effect of surfactant concentration on the formation and droplet size of the emulsions. The droplet size distribution and average droplet diameters of nano-emulsions with different surfactant concentrations were presented in Figs. 3 and 4. We can conclude that with the increase of the surfactant concentration, the droplet size distribution becomes narrow, and the initial average radius of the droplets declines from about 145 to 54 nm as the surfactant concentration increases from 3.0 to 8.0 wt%. This is because the amount of surfactant determines the total interfacial area and hence the average size of the emulsion droplets [13,25].

3.3. Long term stability

The changes in droplet size as a function of the storage time for nano-emulsions with different surfactant concentrations are shown in Fig. 5. Emulsion with 3.0 wt% surfactants flocculated in ten days (data not shown here). We can see from Fig. 5 that samples with surfactant concentration from 4.0 to 8.0 wt% all exhibit good stability. The droplet size grows very slowly, and the growth rate decrease with increasing surfactant concentration, i.e., the stability of the emulsions is improved.

As nonequilibrium systems, emulsions have a tendency to reduce their interfacial areas and free energy through several

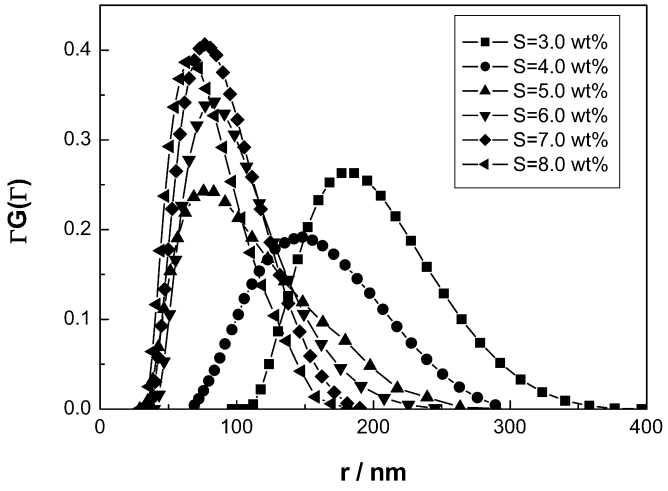

Fig. 3. Droplet size distributions for samples with 20.0 wt% paraffin oil and different surfactant concentrations prepared at 50 °C at an HLB number of 10.3.

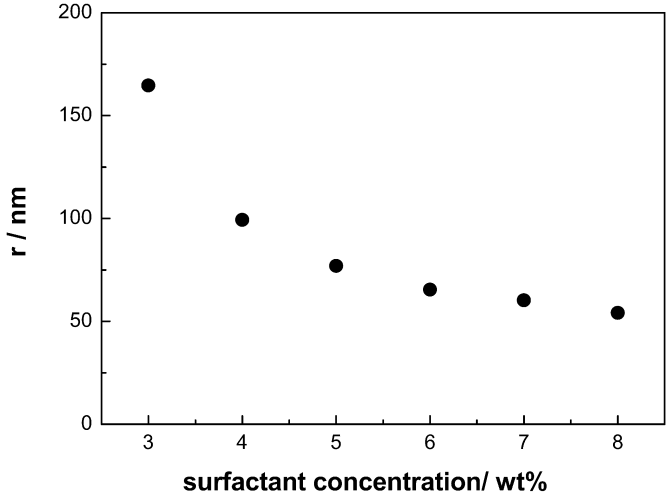

Fig. 4. Radius of droplet as a function of surfactant concentration for samples with 20.0 wt% paraffin oil prepared at 50 °C at an HLB number of 10.3.

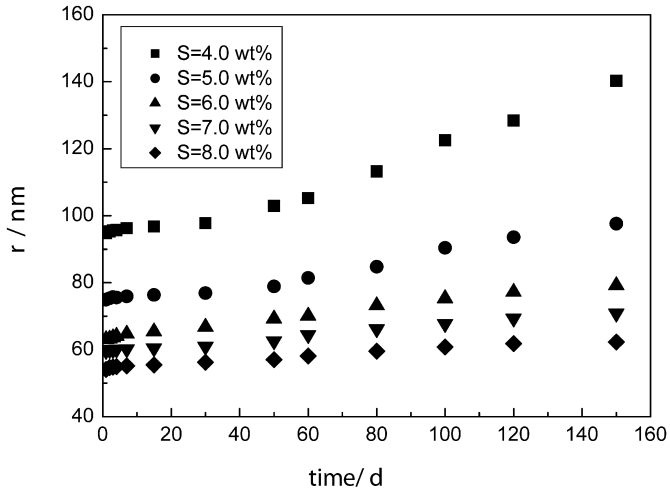

Fig. 5. Radius of droplet as a function of time for samples with 20.0 wt% paraffin oil and different surfactant concentrations.

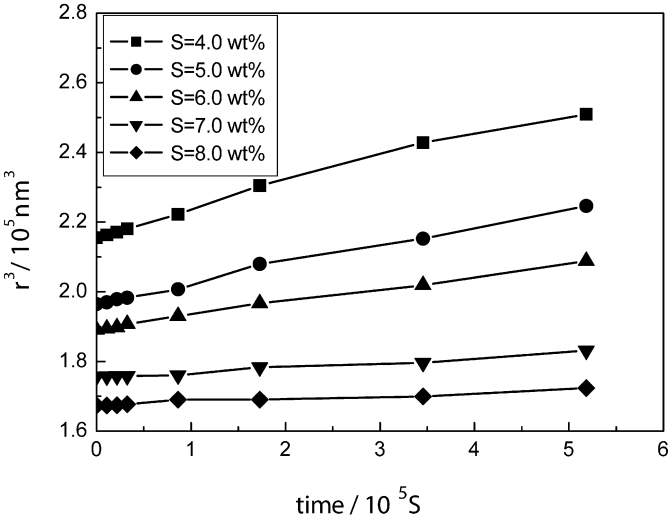

Fig. 6. r^3 of nano-emulsions as a function of time for samples with 20.0 wt% paraffin oil and different surfactant concentrations. For clarity the data have been translated along the ordinate by -6.5×10^5, -2.5×10^5, -0.9×10^5, -0.4×10^5 nm^3 for samples with surfactant concentration of 4.0, 5.0, 6.0 and 7.0 wt%, respectively.

breakdown processes, such as creaming/sedimentation, flocculation, Ostwald ripening and coalescence [1,19]. Compared to conventional emulsions, nano-emulsions often possess good stability against creaming/sedimentation, flocculation, and coalescence because of their small size [1,18,19]. And Ostwald ripening is always found to be the main mechanism producing instability of nano-emulsions [1,18,19,25].

Ostwald ripening arises from the difference in solubility between droplets with different sizes. In this process, larger droplets grow at the expense of smaller ones due to molecular diffusion through the continuous phase. The rate of Ostwald ripening, ω can be obtained by LSW (Lifshitz–Slesov–Wagner) theory [18,19]:

$$\omega = \mathrm{d}r^3/\mathrm{d}t = 8/9\big[(C_\infty \gamma V_m D)/\rho RT\big], \tag{3}$$

where r is the average radius of droplets, t is the storage time, C_∞ is the bulk phase solubility, γ is the interfacial tension between the dispersed phase and medium, V_m is the molar volume of the dispersed phase, D is the diffusion coefficient of the dispersed phase in the continuous phase, ρ is the density of the oil, R is the gas constant and T is the absolute temperature.

Equation (3) implies a linear relationship between the cube of the radius r^3 and time t. We plotted the r^3 of nano-emulsions with different surfactant concentrations as a function of time t in 7 days (the viscosity changed little for these samples, which means no flocculation in 7 days), and found good linear dependence, as shown in Fig. 6. This indicates that the main instability process in our systems is Ostwald ripening. From the slope of each straight line we can calculate the Ostwald ripening rate (listed in Table 3). It is shown that the Ostwald ripening rate declines gradually with the increase of surfactant concentration. This phenomenon is opposite to most results reported in the literatures [13,18–20], which show an increase in the ripening rate with increasing surfactant concentration. This phenomenon is always explained by the presence of surfactant

Table 3
Surfactant concentrations, C_S, initial radius, r_0, and Ostwald ripening rate, ω, for samples with 20.0 wt% paraffin oil at 25 °C

Emulsion	C_S (wt%)	r_0 (nm)	ω ($m^3\,s^{-1} \times 10^{29}$)
1	4.0	95	7.10
2	5.0	74	5.45
3	6.0	65	3.84
4	7.0	60	1.42
5	8.0	54	0.90

micelles in water, which solubilize the oil molecules diffusing in the continuous phase. The bulk oil solubility C_∞ in Eq. (3) is replaced by the concentration of oil solubilized by the micelles, and the micellar diffusion coefficient is instead of the molecular one. This treatment will yield the Ostwald ripening rate in the presence of micelles, predicting a remarkable increase of the rates [18,19]. However, Smet et al. [27] and Hoang et al. [28] observed a reduced ripening rate with increasing surfactant concentration. They argued that the oil solubilized in the micelles was not dispersed at the molecular level in the continuous phase. Since the main rate-determining step in the Ostwald ripening process is oil transport by diffusion of single oil molecules through the continuous phase, the approach of replacing the bulk solubility C_∞ by the total concentration of oil solubilized by micelles is misleading. Surfactant micelles withdraw oil from the emulsion droplets but they do not mediate mass transfer between droplets. That is to say, the oil in the micelles does not contribute to the Ostwald ripening process. As a result, the increase of the amount of micelles actually lowers the term C_∞ in Eq. (3) and hence the ripening rate [27].

In order to determine whether there are micelles present in the continuous phase, we calculated the surfactant concentration required to cover the O/W interface completely. The number of moles n_s of surfactant needed to cover the water/oil interface of an oil volume V is estimated by the following equation [27]:

$$n_s = \frac{3V}{r_0 A N_A}, \tag{4}$$

where a_0 is the initial average particle radius, A is molecular area of the surfactant, N_A is Avogadro's number. According to the literatures, the molecular weight and molecular area of Span 80 (A_S) is 429 g mol^{-1} and 0.46 nm^2, respectively [22]. The molecular weight and molecular area of Tween 80 (A_T) is 1310 g mol^{-1} and 2.48 nm^2, respectively [23]. Here we suppose that the ratio of Tween 80/Span 80 at the O/W interface is equal to their initial ratio (0.44/0.56) in the system, then we can calculate the average molecular weight and molecular area of the mixed surfactants (A_{mix}) by:

$$M_{\text{mix}} = M_T n_T + M_S n_S, \tag{5}$$

$$A_{\text{mix}} = (A_T n_T + A_S n_S), \tag{6}$$

where n_T and n_S are the mole fraction of Tween 80 and Span 80 in the mixed surfactant, respectively. The calculated M_{mix} and A_{mix} are about 688 g mol^{-1} and 1.06 nm^2, respectively.

Substitution of r_0, M_{mix}, A_{mix} into Eq. (4), gives a minimum surfactant concentration about 0.7 wt% for emulsion 1, 1.0 wt% for emulsion 2–4, and 1.2 wt% for emulsion 5. This implies that for emulsion 1–5, there must be enough surfactants left after complete coverage of the O/W interface to form micelles in water, which will withdraw oil molecules diffusing in the continuous phase to lower the Ostwald ripening rate. With the increase of surfactant concentration, the amount of micelles in the continuous phase grows up, which is responsible for the reduced Ostwald ripening rate.

Furthermore, as mentioned above, emulsions with 3.0 wt% surfactants flocculated in ten days. And when we tried to extend the straight lines of r^3 vs t in Fig. 6 to longer time (5 months), we found a deviation between the experiment data and the straight line for each sample, which was reduced with the increase of surfactant concentration. We assume that flocculation may play a role in the destabilization of emulsions during long-term storage process. Larger flocs formed by two or more droplets as a result of flocculation are more susceptible to aggregation than single small droplets, thus accelerating the increase in the droplet size. As the surfactant concentration rises, the droplet size is reduced, causing an increase in the ratio of surfactant film thickness to droplet radius. The relative thicker surfactant film can afford better steric stabilization against flocculation [1], and lowers the impact of flocculation on the instability process.

3.4. Electrophoretic properties

As discussed above, flocculation may contribute to the instability of the nano- emulsions during storage, especially for the samples with low surfactant concentration. Generally, the influence of flocculation can be reduced or eliminated by steric stabilization or by electrostatic stabilization [18]. In our system, the steric stabilization can be achieved by increasing the surfactant concentration, which has been discussed in Section 3.3. The other method to avoid flocculation is to supply enough electrostatic energy barrier between droplets. So we investigated the electrophoretic properties of the nano-emulsions.

The droplets of the nano-emulsions are found to be negatively charged, as shown in Fig. 7. We can see that the zeta potential is approximately −30 mV for the original emulsions at pH 6.8. The zeta potential is strongly dependent on the pH of the system. The absolute value of zeta potential is reduced with of the decrease of pH. At pH 3.8, the zeta potential is close to zero, after which the droplets are positive charged. With the addition of NaOH, the absolute value of the zeta potential increases gradually to −60 mV at pH 9.8 with increasing pH, then it reaches a plateau.

The origin of the negative surface charges on the nonpolar oil droplets has been discussed previously. Ho and Ahmad [29] proposed that the high negative charges on palm olein droplets covered by Emulgen 906 was a result of the adsorption of hydroxyl ions at the O/W interface, due to hydrogen bonding to the EO groups of the Emulgen 906. Hsu and Nacu [30] observed a similar phenomenon in a soybean oil-in-water emulsion stabilized by nonionic Tween series surfactants. However,

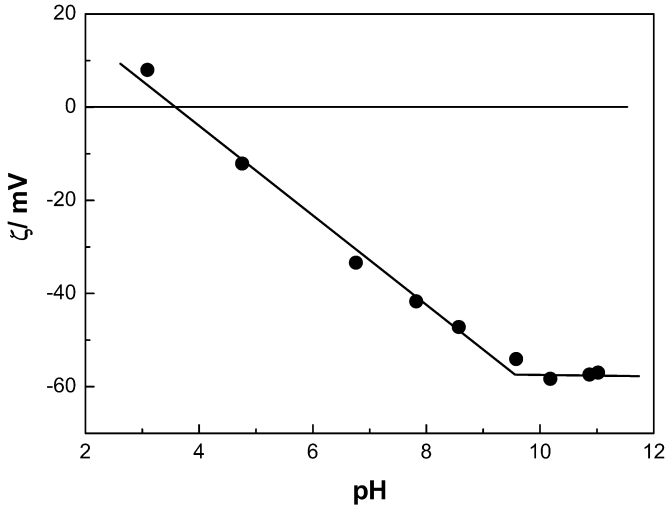

Fig. 7. Zeta potential as a function of pH at 25 °C for samples with 20.0 wt% paraffin oil and 5.0 wt% surfactants.

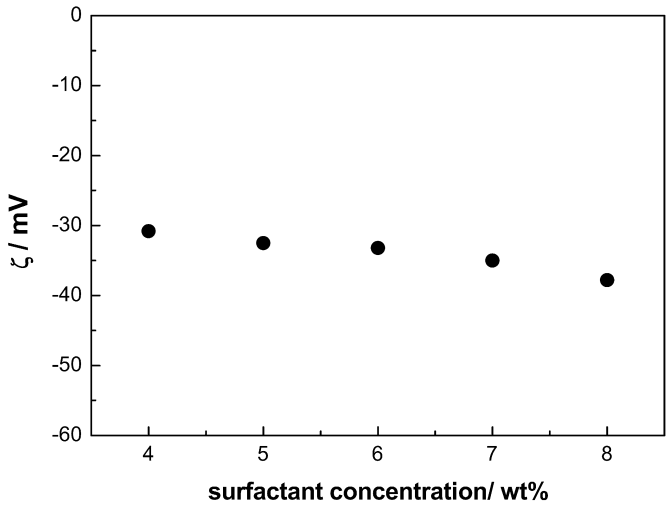

Fig. 8. Zeta potential as a function of surfactant concentration for samples with 20.0 wt% paraffin oil at 25 °C.

Marinova et al. [31] and Stachurski et al. [32] found that hydrocarbon oil drops dispersed without any emulsifier in aqueous phase were also negatively charged. The probable reason for the negative surface charges was suggested to be the specific adsorption of the hydroxyl ions due to the hydrogen bond formation between the hydroxyl ions and water molecules in the boundary layer. Marinova et al. [31] also observed that the magnitude of the zeta potential was reduced when an ultra-pure nonionic surfactant $C_{16}(OE)_8$ was added to the system, indicating that surfactant adsorption at the interface would diminish the area available for the adsorption of hydroxyl ions.

In our system, the nonpolar oil droplets are covered with a mixture of Tween 80 and Span 80. In order to investigate the influence of the nonionic surfactants on the origin of the surface charges, we measured the zeta potential of the droplets as a function of the surfactant concentration (Fig. 8). A slight increase of the absolute zeta potential occurs with increasing surfactant concentration, which contrasts with the results reported by Marinova et al. [31]. Thus, we suggest that the negative charges on the droplets come from the adsorption of hydroxyl ions at the O/W interface, and the EO groups of Tween 80 may create hydrogen bonds with the hydroxyl ions to give more negative surface charges.

It has been reported that the increase of the surface charge can improve the stability of emulsions remarkably [32]. This is because the surface charges can produce repulsive forces between droplets against flocculation and coalescence. In the systems studied, we observed a great increase in the surface charges on the droplets when increasing the pH to a critical value (pH 9.8). As discussed in Section 3.3, flocculation may participate in the instability of nano-emulsions during long-term storage process. So we expect that higher surface charges will enhance the long-term stability against flocculation by tuning the pH of the systems, and plan to investigate this further.

4. Conclusions

Paraffin oil-in-water nano-emulsions have been obtained by EIP method by adjusting the HLB values of the mixed surfactants Tween 80/Span 80. The main instability mechanism for the nano-emulsions has been found to be Ostwald ripening, with a reduced ripening rate as the surfactant concentration rises. This phenomenon may be explained by the surfactant micelles present in the system, which withdraw oil from the continuous phase, lowering the actual solubility of oil in water. In addition, flocculation may contribute to the destabilization of the nano-emulsions during the long-term storage process. We expect the effect of flocculation can be reduced or eliminated by improving the negative surface charges on the droplets through tuning pH of the systems.

Acknowledgments

Financially support from the National Natural Science Foundation of China (No. 20373036) is gratefully acknowledged. The authors also acknowledge Dr. Pamela Holt for her comments on this manuscript.

References

[1] T. Tadros, P. Izquierdo, J. Esquena, C. Solans, Adv. Colloid Interface Sci. 108–109 (2004) 303.
[2] C. Solans, P. Izquierdo, J. Nolla, N. Azemar, M.J. Garcia-Celma, Curr. Opin. Colloid Interface Sci. 3–4 (2005) 102.
[3] C.D. Anderson, E.D. Sudol, M. El-Aasser, Macromolecules 35 (2) (2002) 574.
[4] M. El-Aasser, E.D. Sudol, JCT Res. 1 (1) (2004) 21.
[5] T. Forster, W.V. Rybinski, A. Wadle, Adv. Colloid Interface Sci. 58 (1995) 119.
[6] H. Sagitani, Kanagawa-ku, Takashimadai, JAOCS (1981) 738.
[7] S. Benita, M.Y. Levy, J. Pharm. Sci. 82 (11) (1993) 1069.
[8] H.L. Rasano, T. Lan, A. Weiss, J.H. Whlttam, W.E.F. Gerbacla, J. Phys. Chem. 5 (1981) 468.
[9] O.S. Aubrun, J.T. Simonnet, F. L'Alloret, Adv. Colloid Interface Sci. 108–109 (2004) 145.
[10] H.S. Kang, S.S. Kwon, B.H. Kim, J. Ind. Eng. Chem. 8 (4) (2002) 348.
[11] K. Meleson, S. Graves, T.G. Mason, Soft Mater. 2–3 (2004) 109.
[12] K. Landfester, J. Eisenblatter, R. Rothe, JCT Res. 1 (2004) 65.

[13] A. Forgiarini, J. Esquena, C. González, C. Solans, Progr. Colloid Polym. Sci. 118 (2001) 184.
[14] K. Shinoda, H. Saito, J. Colloid Interface Sci. 26 (1968) 70.
[15] A. Forgiarini, J. Esquena, C. Gonzalez, C. Solans, Langmuir 17 (2001) 2076.
[16] P. Fernandez, V. André, J. Rieger, A. Kühnle, Colloids Surf. A 251 (2004) 53.
[17] L. Dai, W. Li, X. Hou, Colloids Surf. A 125 (1997) 27.
[18] I. Capek, Adv. Colloid Interface Sci. 107 (2004) 125.
[19] P. Taylor, Adv. Colloid Interface Sci. 106 (2003) 261.
[20] P. Izquierdo, J. Esquena, T.F. Tadros, C. Dederen, M.J. Garcia, N. Azemar, C. Solans, Langmuir 18 (2002) 26.
[21] T.C. Ju, C.W. Frank, A.P. Gast, Langmuir 8 (1992) 2165.
[22] L.J. Peltonen, J. Yliruusi, J. Colloid Interface Sci. 227 (2000) 1.
[23] Md.E. Haque, A.R. Das, S.P. Moulik, J. Colloid Interface Sci. 217 (1999) 1.
[24] P.A. Winsor, Chem. Rev. 68 (1968) 1.
[25] D. Morales, J.M. Gutierrez, M.J. Garcia-Celma, C. Solans, Langmuir 19 (2003) 7196.
[26] G. Chen, D. Tao, Fuel Process. Technol. 86 (2005) 499.
[27] Y.D. Smet, L. Deriemaeker, R. Finsy, Langmuir 15 (1999) 6745.
[28] T.K.N. Hoang, V.B. La, L. Deriemaekera, R. Finsy, Langmuir 17 (2001) 5166.
[29] C.C. Ho, K. Ahmad, J. Colloid Interface Sci. 216 (1999) 25.
[30] J.P. Hsu, A. Nacu, J Colloid Interface Sci. 259 (2003) 374.
[31] K.G. Marinova, R.G. Alargova, N.D. Denkov, O.D. Velev, D.N. Petsev, I.B. Ivanov, R.P. Borwankar, Langmuir 12 (8) (1996) 2045.
[32] J. Stachurski, M. Michalek, J. Colloid Interface Sci. 184 (1996) 433.